Supporting Information for "Estimation of the Growth and Dissolution Kinetics of Ammonium Bicarbonate in Aqueous Ammonia Solutions from Batch Crystallization Experiments. 2. The Effect of Sulfate Impurity"

Federico Milella, Marco Mazzotti*

Institute of Process Engineering, ETH Zurich, 8092 Zurich, Switzerland

Abstract

This is the *Supporting Information* to the article "Estimation of the Growth and the Dissolution Kinetics of Ammonium Bicarbonate in Aqueous Ammonia Solutions from Batch Crystallization Experiments. Part II. The Effect of Sulfate Impurity". This document provides:

1. ATR-FTIR calibration standards for the determination of the ammonium bicarbonate concentration in aqueous ammonia solutions containing ammonium sulfate;
2. Micrographs of the populations of seed crystals used in the growth experiments;
3. Crystal size distribution of the final crystallization products;
4. XRD patterns of the final crystallization products;
5. Identifiability of the parameter set of the adsorption-growth model;
6. Assay procedure for the quantification of the sulfate ions' concentration in ammonium bicarbonate samples;
7. Raman spectroscopy characterization of an aqueous ammonia solution containing ammonium bicarbonate and ammonium sulfate.

ATR-FTIR calibration standards for the determination of the ammonium bicarbonate concentration in aqueous ammonia solutions containing ammonium sulfate

The set of standard ammonium bicarbonate (BC) concentrations used for the ATR-FTIR calibration procedure [1] are reported in Table 1 together with the solvent composition (i.e. the aqueous

*I am corresponding author
Email address: marco.mazzotti@ipe.mavt.ethz.ch (Marco Mazzotti)

ammonia and the ammonium sulfate concentrations).

Fig. 1 shows the ammonium bicarbonate solubility relative to the different solvent compositions investigated as well as the different BC standard concentrations used for the calibrations. The ammonia concentration in the solvent is indicated as a weight percent, while the ammonium bicarbonate and ammonium sulfate concentrations are espressed on a molality basis. It is worth noting that both the supersaturated and the undersaturated regions of the phase diagram have been explored during the ATR-FTIR calibration procedure.

	Concentration [mol/kg$_w$]				**Temperature** [°C]			
Solute Sample No.	1	2	3	4	1	2	3	4
NH_4HCO_3 (aq) ($\omega^\circ_{NH_3} = 0$ %, $m^\circ_{AS} = 0$ m)	2.01	2.32	2.52	2.65	5 - 25	10† - 25	10† - 25	16† - 25
NH_4HCO_3 (aq) ($\omega^\circ_{NH_3} = 0$ %, $m^\circ_{AS} = 0.1$ m)	2.01	2.56	2.72	n/a	6† - 25	10† - 22	20† - 25	n/a
NH_4HCO_3 (aq) ($\omega^\circ_{NH_3} = 0$ %, $m^\circ_{AS} = 0.3$ m)	1.89	2.13	2.72	n/a	5 - 27	5† - 28	10† - 25	20† - 29
NH_4HCO_3 (aq) ($\omega^\circ_{NH_3} = 2$ %, $m^\circ_{AS} = 0$ m)	2.64	2.89	3.05	3.17	5 - 25	8† - 25	12† - 25	14† - 25
NH_4HCO_3 (aq) ($\omega^\circ_{NH_3} = 2$ %, $m^\circ_{AS} = 0.2$ m)	2.50	2.95	3.27	n/a	5 - 25	7† - 25	15† - 25	n/a
NH_4HCO_3 (aq) ($\omega^\circ_{NH_3} = 2$ %, $m^\circ_{AS} = 0.4$ m)	2.50	2.85	2.95	3.28	6† - 25	5 - 25	12† - 25	16† - 25

Table 1: Set of ammonium bicarbonate standard concentrations in aqueous ammonia solutions containing ammonium sulfate and relative temperature range adopted (see Fig. 1); the variable $\omega^\circ_{NH_3}$ refers to the nominal ammonia concentration in the solvent in percent weight, the concentration of ammonium bicarbonate and ammonium sulfate are indicated using a molality basis. The symbol (†) refers to the temperature value corresponding to the onset of primary nucleation.

Micrographs of the populations of seed crystals used in the growth experiments

Two different batches of BC seed crystals have been used in this work, namely seeds type A and type B. They have been obtained by temperature cycles performed on ammonium bicarbonate crystals recrystallized from a supersaturated aqueous solution of BC. The size ranges obtained were between 100−250 µm for seeds A, and between 150−350 µm for seeds B. Fig. 2 shows the corresponding micrographs of the seed populations. Note that the difference in final appearance of the two types of crystals stems from the specific production process of the crystals. In the case of type A seeds the temperature cycles terminated with a cooling step, while in the case of type B seeds the production process ended with a heating step (hence the more rounded shape of the crystals).

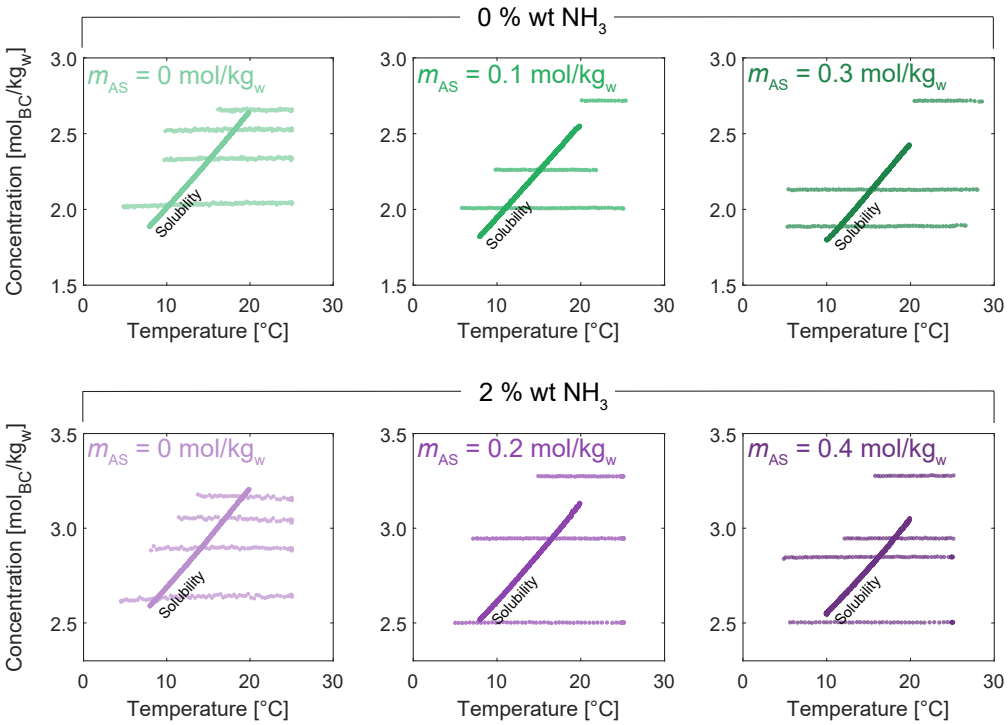

Figure 1: Graphical representation of the ATR-FTIR calibration sets. The temperature range is 5-29 °C. The solubility curve, highlighted in the graphs, separates the supersaturated region from the undersaturated region of the phase diagram. The nominal ammonia concentration in the solvent is indicated as a weight percent, while m_{AS} is the nominal concentration of ammonium sulfate is indicated as a molality basis (water being the solvent). Note that the different color codes, green and purple, indicate the different nominal ammonia concentrations in the solvent, i.e. 0 % wt or 2 % wt respectively, while the increasing color intensity indicates increasing concentration of ammonium sulfate in solution.

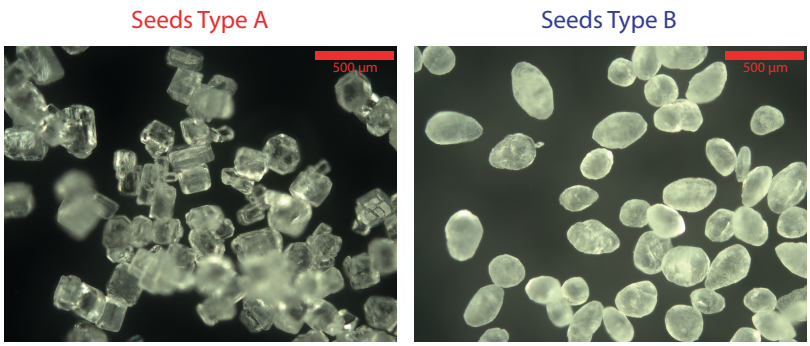

Figure 2: Micrographs of the populations of seed crystals used in this work.

Crystal size distribution of the final crystallization products

Fig. 3 shows the normalized volume-weighted crystal size distribution (CSD) of the ammonium bicarbonate crystals, n_{v}, obtained after the growth experiments reported in Table 2 in the article. The CSDs have been sampled using the μ-DISCO [2] and have been compared with the initial seed distributions (shown in gray color). The measurements have been carring out by suspending the crystals in an solution of ethanol (saturated with BC), acquiring 1600 images per measurement every 2 min until the cumulative number of sampled particles reached a value above 30,000.

Identifiability of the parameter set of the adsorption-growth model

In this section, the practical identifiability [3] of the kinetic parameter set of the adsorption-growth model proposed in this work is discussed.

The correlation among the Langmuir constant, κ, and the impurities effective factor, α, which constitute the model parameters, have been studied by analyzing the behavior of the objective function, Ψ, defined as

$$\Psi = \frac{N_{\mathrm{t}}}{2} \ln \left[\sum_{j=1}^{N_{\mathrm{t}}} \left(\frac{m_{\mathrm{BC},j} - \hat{m}_{\mathrm{BC},j}(\mathbf{p})}{m^{\mathrm{ref}}} \right)^2 \right] \tag{1}$$

where the index j indicates the j-th experimental concentration data points relative to the growth experiments reported in Table 2 in the article, and $\hat{m}_{\mathrm{BC},j}$ is the model response that depends on the vector parameter $\mathbf{p} = [\kappa, \alpha]$.

The isocontour curves of the objective function Ψ, parametrized with respect to the model parameters κ and α are shown in Fig. 4. The presence of a locus of points in which the function is minized, rather than a unique point, is representative of the statistical correlation among the parameters. In turn, this means that *only* relative values of the model parameters can be identify, without being able to determine accurately the value of each individual parameter.

As discussed in the article, the parameters' non-identifiability has been removed by arbitrarily setting the value of α to 1, hence performing a parameter fitting based on the parameter κ, the only adjustable parameter of the model.

XRD patterns of crystal products obtained from the growth experiments

The nature of the crystals obtained from the desupersaturation growth experiments reported in Table 2 in the article was verified by analyzing the powder X-ray diffraction patterns (XRDP)

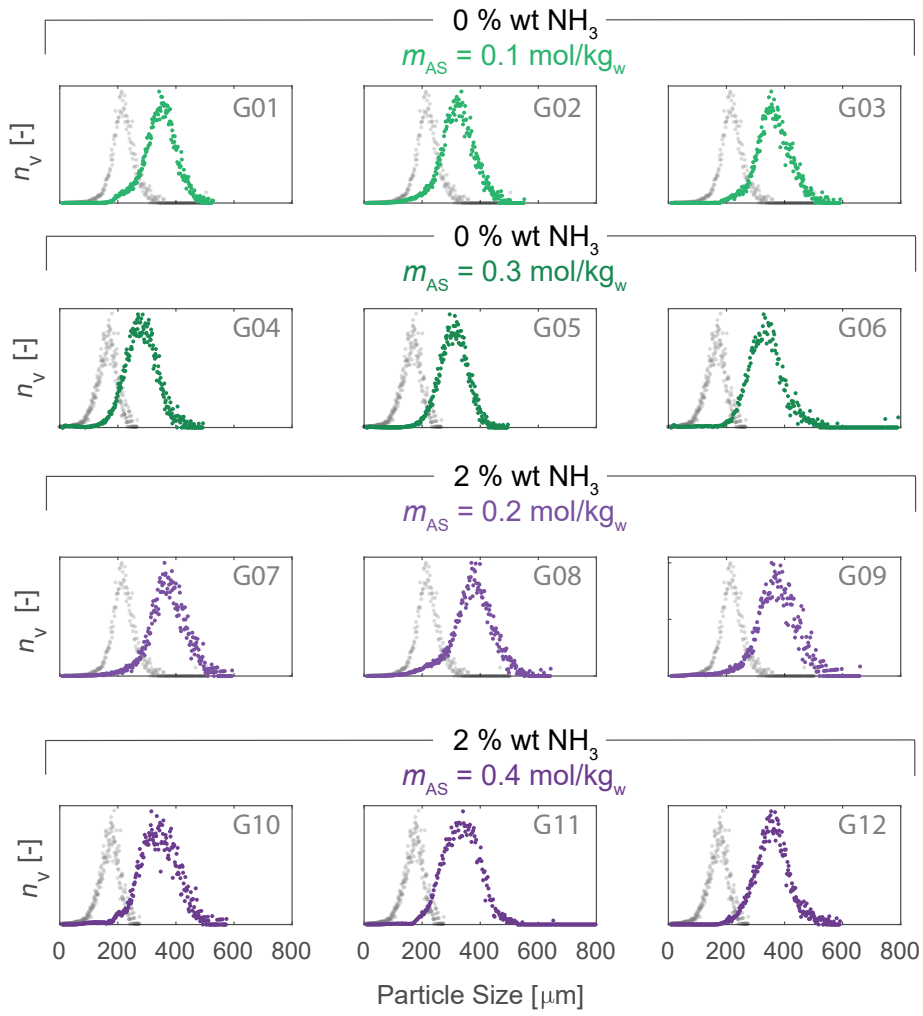

Figure 3: Normalized volume-weighted crystal size distribution (CSD) of the ammonium bicarbonate crystals, n_v, obtained after the growth experiments reported in Table 2 in the article. The nominal ammonia concentration in the solvent is indicated as a weight percent, while m_{AS} is the nominal concentration of ammonium sulfate indicated as a molality basis (water being the solvent). Note that the different color codes, green and purple, indicate the different nominal ammonia concentrations in the solvent, i.e. 0 % wt or 2 % wt respectively, while the increasing color intensity indicates increasing concentration of ammonium sulfate in solution.

of the solid phase shown in Fig. 5. The XRDP were recorded after samples were spread uniformly over the sample holder using a diffractometer from Bruker (D2 Phaser, 30 kV, 10 mA, Cu KR; Karlsruhe, Germany). Patterns were recorded at 2θ between 10° and 80° with resolution of 0.02° and a scan speed of $5.83\,^{\circ}\,\mathrm{min}^{-1}$.

The X-ray patterns of the crystal products match qualitatively with the one of pure ammonium

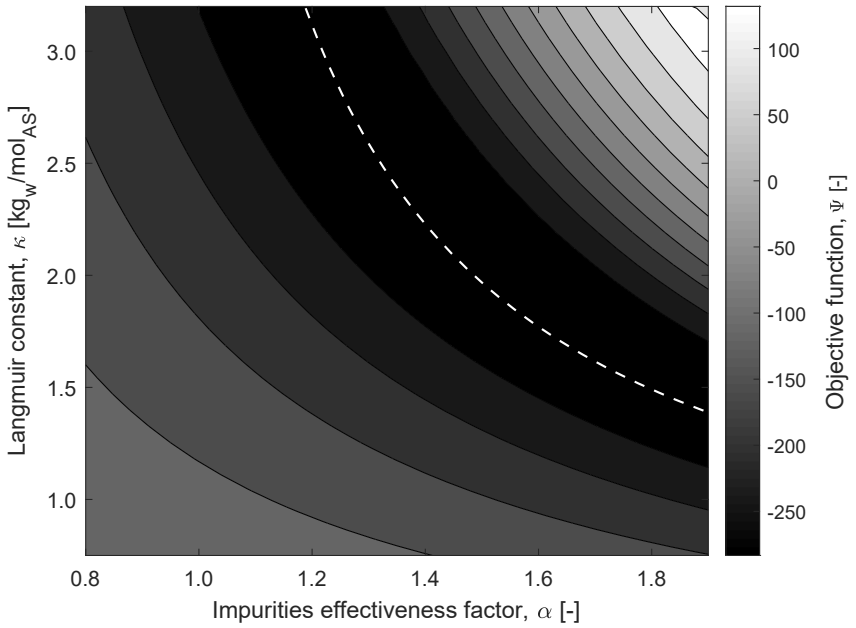

Figure 4: Indentifiability of the adsorption-growth model parameters. The isocontour lines of the objective function Ψ (Eq. 1) have been computed by varying the values of the Langmuir constant, κ, and of the impurities effective factor, α, of the adsorption-growth model. Dashed white line indicates the minimum values of the objective function Ψ.

bicarbonate (black pattern in Fig. 5). The XRPD of pure ammonium sulfate is shown as reference in red.

Assay procedure for the quantification of the sulfate ions' concentration

The procedure involved an extensive washing of the BC crystals with ethanol saturated w.r.t. BC in order to remove any mother liquor adhering to the surface of the crystals. After drying, few grams of BC crystals have been dissolved in an aqueous solution (Milli-Q water). Prior to the addition of $BaCl_2$(aq) to the solution in order to precipitate $BaSO_4$ (that would occur only in presence of ${SO_4}^{2-}$ ions), all the carbon species have been removed to avoid the concomitant precipitation of $BaCO_3$, which is also sparingly soluble in water. This has been achieved by lowering the pH of the solution by means of an addition of HCl(aq) to the sample. As a consequence of the decrease in pH value, the carbon distribution shifted towards pure CO_2(aq) that was easily stripped away from the solution by degassing it in a vacuum oven at 50 °C for about 5 h. Then, the pH of the carbon-free solution has been adjusted to a value of 9 (by adding a NaOH(aq)) so that the sulfur

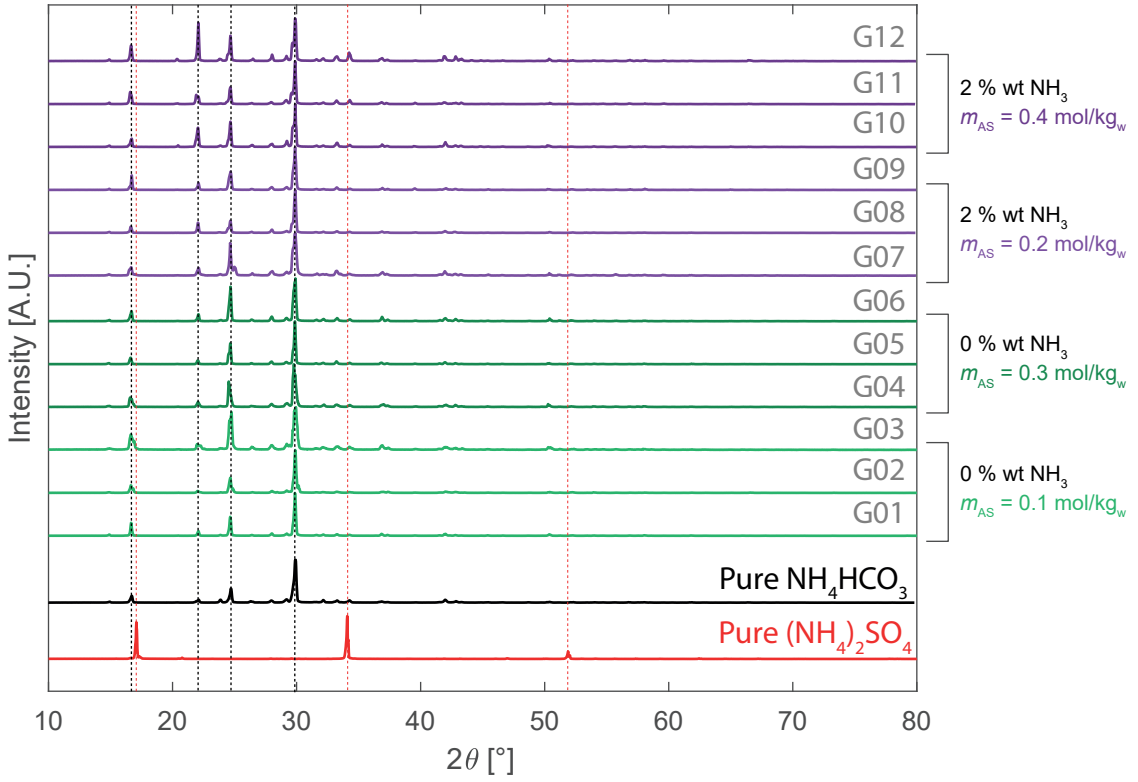

Figure 5: X-ray diffraction patterns of the crystallization products obtained from the desupersaturation growth experiments reported in Table 2 in the article. The X-ray diffraction patterns of pure ammonium bicarbonate and pure ammonium sulfate are shown as reference in black and red color, respectively.

species would be present only as SO_4^{2-} ions [6].

After the addition of $BaCl_2$(aq) in stoichiometric eccess, the suspensions were left settling for 24 h. The solids that eventually precipitated were recovered by filtering the suspension (using a 47 mm, 0.45 µm pore size cellulose nitrate filter) and analyzed through PXRD measurements to identify the nature of the crystalline phase. The PXRD solid sample has been prepared by collecting all the precipitated solid from the 12 samples (each one from a different crystallization experiment, cf. Table 2 of the article) into a single sample that has been ground before the analysis.

An AX205 analytical balance (Mettler-Toled, Switzerland) with a readability and maximum capacity of 0.01 mg and 81 g, respectively has been used to weigh the the amount of precipitated $BaSO_4$.

Fig. 6 shows the PXRD analysis on the solids precipitated during the assays (black curve) and the comparison with the reference XRDP of barium sulfate [4] (red curve) and of barium carbonate [5]

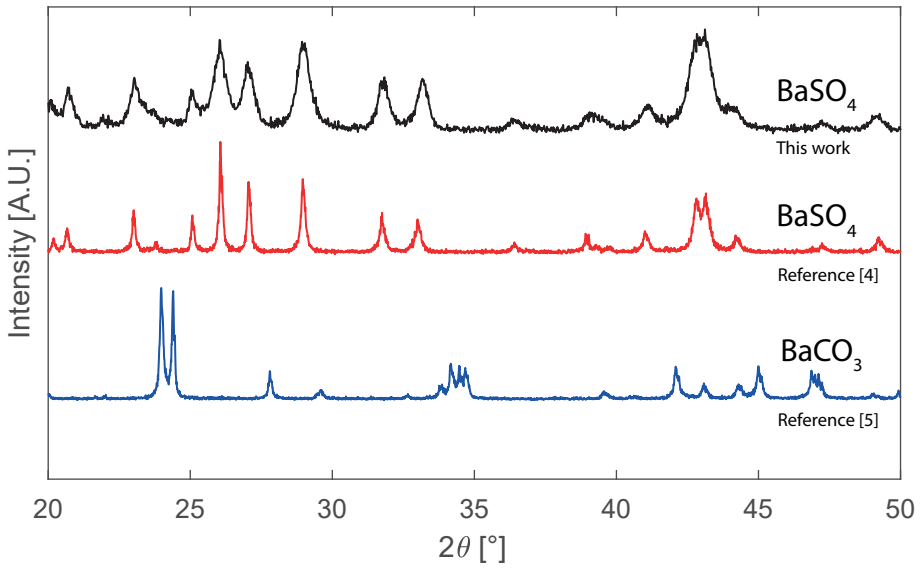

Figure 6: X-Ray diffraction patterns (XRDP) of the solid phase precipitated during the sulfate assay. The PXRD solid sample has been prepared by collecting all the precipitated solid from the 12 samples (each one from a different crystallization experiment, cf. Table 2 of the article). The XRDP of barium sulfate [4] (red curve) and of barium carbonate [5] (blue curve) are reported as reference.

(blue curve). As it can be seen from Fig. 6, the compound precipitated during the assay was barium sulfate.

Raman spectroscopy characterization of an aqueous ammonia solution containing ammonium bicarbonate and ammonium sulfate

In this work, the Raman spectrum of an aqueous ammonia solution containing ammonium bicarbonate and ammonium sulfate (nominal concentrations of ammonia, ammonium bicarbonate, and ammonium sulfate, equal to 2 % wt, 2.95 m_{BC}, and 0.2 m_{AS}, respectively) has been analyzed to investigate the presence of anomalies in the Raman shift modes that could be related to the presence of ion-paring or to the formation of ion complexes in solution. It must be noted that we refrained from generalizing the findings of this cursory analysis, which only serves the purpose of investigating the chemical composition of the mixture.

A RA 400 Raman spectrometer from Mettler-Toledo (Greifensee, Switzerland) equipped with a 250 mW frequency-stabilized laser diode at 785 nm and a thermoelectrically cooled CCD detector

Species	**Position**	**Width**	**Height**
	[cm^{-1}]	[cm^{-1}]	[A.U.]
Sulfate ion ($SO_4{}^{2-}$)	981 [8]	10.21	480.2
Carbamate ion (NH_2COO^-)	1020 [9]	31.55	515.1
Bicarbonate ion ($HCO_3{}^-$)	1037 [9]	14.33	462.3
Carbonate ion ($CO_3{}^{2-}$)	1066 [9]	13.55	300.0

Table 2: Optimal parameter of the Raman peaks of each species present in solution. Note that the peak position of each compound has been taken from literature data.

was used. In situ measurements were recorded using a 5/8 in. ball-type immersion probe (Inphotonics, Norwood, MA) connected via a fiber optic (thicknesses of collection and excitation fibers were 100 and 200 µm, respectively) in a thermostated reactor at the temperature of 25 °C. The Raman spectra were collected at a laser intensity of 150 mW in the range 190 to 1150 cm^{-1} with a resolution of 0.5 cm^{-1} and were averaged over 10 scans using an exposure time of 5 s.

At first, the Raman spectum recorded during the measurement of the aforementioned mixture has been post-processed by applying a *linear baseline* correction in the range 190 to 1150 cm^{-1}. Then, the measured spectrum of the mixture, indicated with purple circular markers in Fig. 7, has been modeled using a least-squares minimization approach. The black solid curve in Fig. 7 represents the result of the fitting procedure and it is obtained by superimposing the contributions of the Raman spectra of the individual species in solution. In detail, the optimization procedure considers the presence of 4 main species, namely the bicarbonate ion, the carbonate ion, the carbamate ion, and the sulfate ion. Multiple Gaussian/Lorentzian blend functions with independently variable percent Gaussian have been used to model each species' spectrum. The calculations have been performed in MATLAB using the open-source software *Peak Fitter* available on-line [7]. Table 2 gives an overview of the optimal parameters for each component modeled during the spectrum fitting.

Fig. 7 shows that the measured spectrum of the mixture can be properly reproduced by a linear combination of the spectra of the species in solution. Based on this evidence, which we refrain from generalizing, we neglected the presence of ionic complexes, in the range of ammonium bicarbonate, ammonium sulfate and aqueous ammonia concentrations investigated in this work as well as in the computation of the ionic equilibria for the $CO_2-NH_3-H_2O-SO_x$ system.

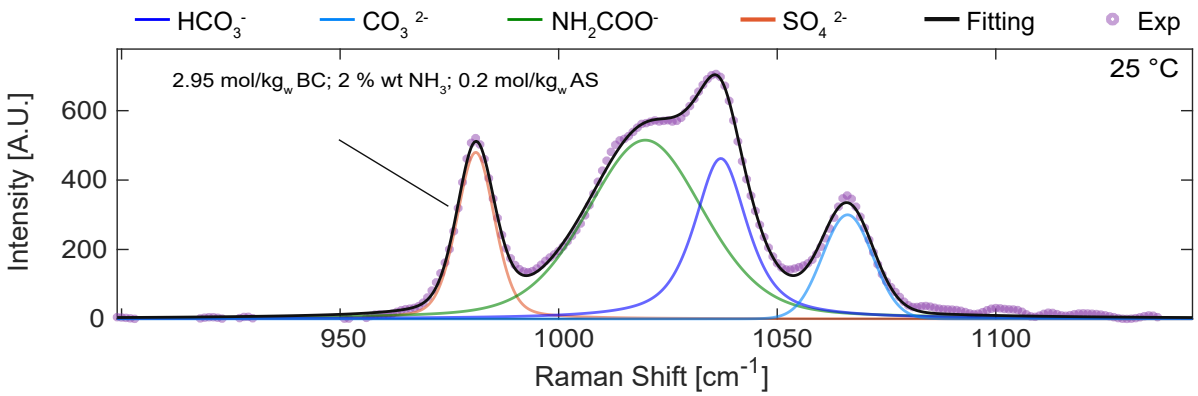

Figure 7: Raman spectrum of an aqueous ammonia solution containing ammonium bicarbonate and ammonium sulfate at the nominal concentrations of ammonia, ammonium bicarbonate, and ammonium sulfate, equal to 2 % wt, 2.95 m_{BC}, and 0.2 m_{AS}, respectively. Data has been recorded at 25 °C. The measured intensities of the measured spectrum, reported in arbitrary unit, are represented by purple circular markers, while the black solid line is the fitted spectrum. The remain spectra are the contributions of each species' spectrum to the fitted Raman spectrum of the mixture.

References

[1] J. Cornel, C. Lindenberg, M. Mazzotti, Quantitative Application of in Situ ATR-FTIR and Raman Spectroscopy in Crystallization Processes, Ind. Eng. Chem. Res. 47 (14) (2008) 4870–4882. doi:10.1021/ie800236v.

[2] A. K. Rajagopalan, J. Schneeberger, F. Salvatori, S. Bötschi, D. R. Ochsenbein, M. R. Oswald, M. Pollefeys, M. Mazzotti, A comprehensive shape analysis pipeline for stereoscopic measurements of particulate populations in suspension, Powder Technol. 321 (2017) 479–493. doi:10.1016/j.powtec.2017.08.044.

[3] R. Brun, P. Reichert, H. R. Künsch, Practical identifiability analysis of large environmental simulation models, Water Resour. Res. 37 (4) (2001) 1015–1030. doi:10.1029/2000WR900350.

[4] University of Arizona Mineral Museum, Baryte powder diffraction x-ray patters, rruff.info/R040036.

[5] University of Arizona Mineral Museum, Witherite powder diffraction x-ray patters, rruff.info/R040040.

[6] J. Casas, F. Alvarez, L. Cifuentes, Aqueous speciation of sulfuric acid–cupric sulfate solutions, Chem. Eng. Sci. 55 (24) (2000) 6223–6234. doi:10.1016/S0009-2509(00)00421-8.

[7] T. O'Haver, Peak fitter, https://terpconnect.umd.edu/ toh/spectrum/InteractivePeakFitter.htm, (2019).

[8] R. Buchner, T. Chen, G. Hefter, Complexity in "Simple" Electrolyte Solutions: Ion Paring in $MgSO_4$(aq), J. Phys. Chem. B 108 (7) (2004) 2365–2375. doi:10.1021/jp034870p.

[9] N. Wen, M. H. Brooker, Ammonium Carbonate, Ammonium Bicarbonate, and Ammonium Carbamate Equilibria: A Raman Study, J. Phys. Chem. 99 (1) (1995) 359–368. doi:10.1021/j100001a054.